Supporting Information:

Environment-driven reactivity of H_2 on PdRu surface alloys

M. Ramos,[1] M. Minniti,[2] C. Díaz,[3] D. Farías,[2] R. Miranda,[2,4]
F. Martín,[3,4] A. E. Martínez,[1] and H. F. Busnengo[1]

[1]*Grupo de Fisicoquímica en Interfases y Nanoestructuras, Instituto de Física Rosario and Universidad Nacional de Rosario, 2000 Rosario, Argentina*

[2]*Departamento de Física de la Materia Condensada, and Instituto Nicolás Cabrera, Universidad Autónoma de Madrid, 28049 Madrid, Spain*

[3]*Departamento de Química, Universidad Autónoma de Madrid, 28049 Madrid, Spain*

[4]*Instituto Madrileño de Estudios Avanzados en Nanociencia (IMDEA-Nanociencia), 28049 Madrid, Spain*

(Dated: July 8, 2013)

EXPERIMENTAL DETAILS

Experiments have been carried out in a Helium Atom Scattering (HAS) apparatus described elsewhere [1]. The angular distribution of the scattered atoms are measured with a quadrupole mass spectrometer mounted on a two–axis goniometer. Details on Ru(0001) surface preparation can be found elsewhere [2]. Surface cleanliness and order was checked using low-energy electron diffraction (LEED) and HAS. In order to detect the specularly reflected He beam in measurements like the one shown in Fig. 1, an angle of incidence different from normal incidence must be used. Therefore, such data have been measured with an angle of incidence $\Theta_i = 15^\circ$, which is the smallest angle which allows detection of specular diffraction, owing to limitations in the rotating system of our detector.

A critical issue in the current experiments is the determination of the Pd coverage. The evaporator has been calibrated by measuring the completion of the first Pd layer on Ru(0001), on which it grows epitaxially [3, 4]. Pd was deposited from a commercial evaporator, using a Pd rod. The quality of evaporated films has been checked by monitoring the intensity of the specular He beam as a function of deposition time taking advantage of the high sensitivity of HAS to surface defects [5, 6]. A typical deposition curve is shown in Fig. SI 1. The maximum observed corresponds to the completion of the first Pd epitaxial layer, which forms when Pd is deposited at a surface temperature of 700 K [3, 4]. The first

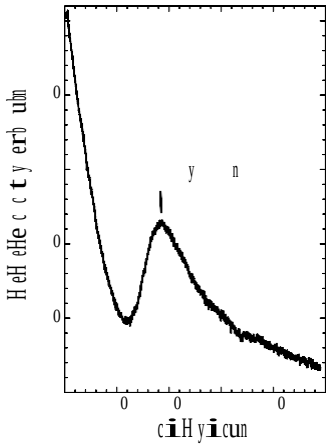

FIG. SI 1. Intensity of the specularly reflected He beam during Pd evaporation on Ru(0001) as a function of time. The evaporation rate is ~ 0.03 ML/min. The surface temperature is 700 K.

maximum in the reflected He specular intensity occurs after about 40 minutes, which corresponds to an evaporation rate of ~ 0.03 ML/min. Thus, with this technique we were able to determine the amount of deposited Pd at intermediate coverages with a daily precision of ca. 1%.

COMPUTATIONAL DETAILS

Let us consider a gas of molecular hydrogen at temperature T_g in contact with a surface. The number of molecules impinging the surface per unit time on a unit area with a center of mass velocity **v**, with spherical coordinates within the ranges $(v,\ v + dv)$; $(\theta_v,\ \theta_v + d\theta_v)$ and $(\varphi_v,\ \varphi_v + d\varphi_v)$, and in a rovibrational state characterized by the quantum numbers (v,J) and energy $E(v,J)$, is [7]:

$$d^3\boldsymbol{f} = n \left(\frac{M}{2\pi k_B T_g}\right)^{3/2} F_B(v, J; T_g)\ \exp\left(-\frac{M v^2}{2k_B T_g}\right) v^3 \cos\theta_v \sin\theta_v dv d\theta_v d\varphi_v. \qquad \text{(SI. 1)}$$

In Eq. SI. 1, $F_B(v, J; T_g)$ is the Boltzmann weight factor,

$$F_B(v, J; T_g) = \frac{w(J) \exp\left(-\frac{E(v,J)}{k_B T_g}\right)}{\sum_{v,J} w(J) \exp\left(-\frac{E(v,J)}{k_B T_g}\right)}, \qquad \text{(SI. 2)}$$

n is the density of molecules in the gas, M the mass of the molecules, and k_B the Boltzmann constant. In addition,

$$w(J) = \begin{cases} (2J+1), & \text{if } J \text{ is even} \\ 3(2J+1), & \text{if } J \text{ is odd} \end{cases} \qquad \text{(SI. 3)}$$

for H_2, and

$$w(J) = \begin{cases} 2(2J+1), & \text{if } J \text{ is even} \\ (2J+1), & \text{if } J \text{ is odd} \end{cases} \qquad \text{(SI. 4)}$$

for D_2.

Accordingly, the thermally averaged initial sticking probability, $s_0(T_g)$, can be computed as follows:

$$s_0(T_g) = \frac{\int_0^{+\infty} dv \int_0^{\pi/2} d\theta_v \int_0^{2\pi} d\varphi_v\ v^3 \cos\theta_v \sin\theta_v \exp\left(-\frac{Mv^2}{2k_B T_g}\right) \bar{s}_0(v,\ \theta_v, \varphi_v)}{\int_0^{+\infty} dv \int_0^{\pi/2} d\theta_v \int_0^{2\pi} d\varphi_v\ v^3 \cos\theta_v \sin\theta_v \exp\left(-\frac{Mv^2}{2k_B T_g}\right)}, \qquad \text{(SI. 5)}$$

where

$$\bar{s}_0(v,\ \theta_v, \varphi_v) = \sum_{v,J} w(J)\ F_B(v, J; T_g)\ s_0(v, \theta_v, \varphi_v, v, J), \qquad \text{(SI. 6)}$$

and $s_0(v,\ \theta_v, \varphi_v, v, J)$ is the rovibrational-state-selective initial sticking probability.

If $\bar{s}_0$ scales with total energy [i.e. $\bar{s}_0(v,\ \theta_v, \varphi_v) = \bar{s}_0(v)$], Eq. SI. 5 reduces to:

$$s_0(T_g) = \frac{\int_0^{+\infty} \exp\left(-\frac{Mv^2}{2k_B T_g}\right) \bar{s}_0(v)\ v^3 dv \int_0^{\pi/2} \cos\theta_v \sin\theta_v d\theta_v \int_0^{2\pi} d\varphi_v}{\int_0^{+\infty} \exp\left(-\frac{Mv^2}{2k_B T_g}\right) v^3 dv \int_0^{\pi/2} \cos\theta_v \sin\theta_v d\theta_v \int_0^{2\pi} d\varphi_v}$$
$$= \frac{\int_0^{+\infty} \exp\left(-\frac{Mv^2}{2k_B T_g}\right) \bar{s}_0(v)\ v^3 dv}{\int_0^{+\infty} \exp\left(-\frac{Mv^2}{2k_B T_g}\right) v^3 dv}. \qquad \text{(SI. 7)}$$

Then, using $Mv^2/2 = E$ $(Mv dv = dE)$, one finally obtains:

$$s_0(T_g) = \frac{\int_0^{+\infty} E \exp\left(-\frac{E}{k_B T}\right) \bar{s}_0(E)\ dE}{\int_0^{+\infty} E \exp\left(-\frac{E}{k_B T}\right) dE}$$
$$= (k_B T_g)^{-2} \int_0^{+\infty} E \exp\left(-\frac{E}{k_B T}\right) \bar{s}_0(E)\ dE. \qquad \text{(SI. 8)}$$

Instead of using spherical coordinates (v, θ_v, φ_v), one can use cylindrical coordinates, $(v_\perp, v_\parallel, \varphi_v)$, being $v_\perp = v\cos\theta_v$ and $v_\parallel = v\sin\theta_v$ the components of $\mathbf{v}$ perpendicular and parallel to the surface respectively $(v^2 = v_\perp^2 + v_\parallel^2)$. Taking into account that for any function $g(\mathbf{v})$,

$$\int_0^{+\infty} v^2 dv \int_0^{\pi/2} \sin\theta_v d\theta_v \int_0^{2\pi} d\varphi_v\ g(v, \theta_v, \varphi_v) =$$
$$\int_0^{+\infty} dv_\perp \int_0^{+\infty} v_\parallel\, dv_\parallel \int_0^{2\pi} d\varphi_v\ g(v_\perp, v_\parallel, \varphi_v), \qquad \text{(SI. 9)}$$

Eq. SI. 5 can be re-written as:

$$s_0(T_g) = \frac{\int_0^{+\infty} v_\perp dv_\perp \int_0^{+\infty} v_\parallel\, dv_\parallel \int_0^{2\pi} d\varphi_v \exp\left(-\frac{M(v_\perp^2 + v_{I\parallel}^2)}{2k_B T_g}\right) \bar{s}_0(v_\perp, v_\parallel, \varphi_v)}{\int_0^{+\infty} v_\perp dv_\perp \int_0^{+\infty} v_\parallel\, dv_\parallel \int_0^{2\pi} d\varphi_v \exp\left(-\frac{M(v_\perp^2 + v_{I\parallel}^2)}{2k_B T_g}\right)}. \qquad \text{(SI. 10)}$$

Eq. SI. 10 is particularly convenient if $\bar{s}_0$ scales with normal energy [i.e. $\bar{s}_0(v_\perp, v_\parallel, \varphi_v) = \bar{s}_0(v_\perp)$], because it can be reduced to:

$$s_0(T_g) = \frac{\int_0^{+\infty} \exp\left(-\frac{Mv_\perp^2}{2k_B T_g}\right) \bar{s}_0(v_\perp)\ v_\perp dv_\perp \int_0^{+\infty} \exp\left(-\frac{Mv_{I\parallel}^2}{2k_B T_g}\right) v_\parallel\, dv_\parallel \int_0^{2\pi} d\varphi_v}{\int_0^{+\infty} \exp\left(-\frac{Mv_\perp^2}{2k_B T_g}\right) v_\perp dv_\perp \int_0^{+\infty} \exp\left(-\frac{Mv_{I\parallel}^2}{2k_B T_g}\right) v_\parallel\, dv_\parallel \int_0^{2\pi} d\varphi_v}$$
$$= \frac{\int_0^{+\infty} \exp\left(-\frac{Mv_\perp^2}{2k_B T_g}\right) \bar{s}_0(v_\perp)\ v_\perp dv_\perp}{\int_0^{+\infty} \exp\left(-\frac{Mv_\perp^2}{2k_B T_g}\right) v_\perp dv_\perp}. \qquad \text{(SI. 11)}$$

Then, using $M v_\perp^2/2 = E_\perp$ ($M v_\perp dv_\perp = dE_\perp$), one finally obtains:

$$s_0(T_g) = \frac{\int_0^{+\infty} \exp\left(-\frac{E_\perp}{k_B T_g}\right) \bar{s}_0(E_\perp)\, dE_\perp}{\int_0^{+\infty} \exp\left(-\frac{E_\perp}{k_B T_g}\right) dE_\perp} = (k_B T_g)^{-1} \int_0^{+\infty} \exp\left(-\frac{E_\perp}{k_B T}\right) \bar{s}_0(E_\perp)\, dE_\perp . \quad \text{(SI. 12)}$$

For simplicity, Eqs. SI. 8 and SI. 12 can be written in a single expression:

$$s_0(T_g) = \int_0^{+\infty} f_B(E_i)\, \bar{s}_0(E_i)\, dE_i \quad \text{(SI. 13)}$$

with

$$f_B(E_i) = (k_B T_g)^{-(\alpha+1)} E_i^{\alpha} \exp\left(-\frac{E_i}{k_B T_g}\right) \quad \text{(SI. 14)}$$

being α equal to 0 or 1 if the sticking probability scales with normal or total energy respectively, and $\bar{s}_0(E_i)$ the thermally averaged (over v, J) rovibrational-state-selective sticking probability for impact energy E_i at normal incidence:

$$\bar{s}_0(E_i) = \sum_{v,J} w(J)\, F_B(v, J; T_g)\, s_0(v = \sqrt{2E_i/M}, \theta_v = 0, v, J). \quad \text{(SI. 15)}$$

In order to compute s_0, in this work we have carried out the so-called quasi-classical trajectory (QCT) calculations in which, the rovibrational energy E(v,J) of molecular hydrogen in vacuum is taken into account for the sampling of the initial conditions (see e.g. ref. [8]).

ELECTRONIC STRUCTURE OF PD_xRU_{1-x}/RU(0001)

In order to rationalize the increasing reactivity of Ru atoms in the Pd_xRu_{1-x}/Ru(0001) alloys with the increase of nearest neighbor (NN) Pd atoms, we have computed the projected density of d-states (PDOS) on a topmost-layer Ru atom of pure Ru(0001), $Pd_{0.11}Ru_{0.89}$/Ru(0001) (we selected a Ru NN of the Pd atom), and $Pd_{0.89}Ru_{0.11}$/Ru(0001) (the Ru atom is surrounded by all Pd atoms). The main features of the three Ru-PDOSs are similar to each other, in particular the width of the d-band. However, comparing the position of the center of the d-band it is observed a small but systematic up-shift with the number of NN Pd atoms: from ~ -1.9 eV for 0 Pd to ~ -1.6 eV for 6 Pds, being these energies defined with respect to the Fermi level of each surface. Thus, the d-band model [9] that predicts direct correlation between reactivity and the height of the d-band center (due to the consequent lower population of anti-bonding metal-adsorbate states) allows one

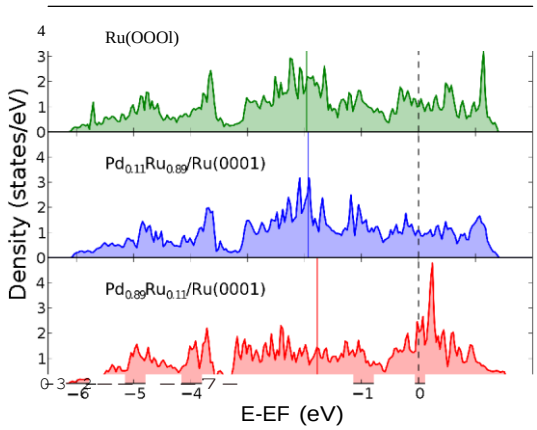

FIG. SI 2. Density of d-states projected on a topmost-layer Ru atom of Ru(OOOl) (top panel), Pdo.uRuo.sg/Ru(OOOl) (middle panel) and Pdo.sgRuo.u/Ru(OOOl) (bottom panel).

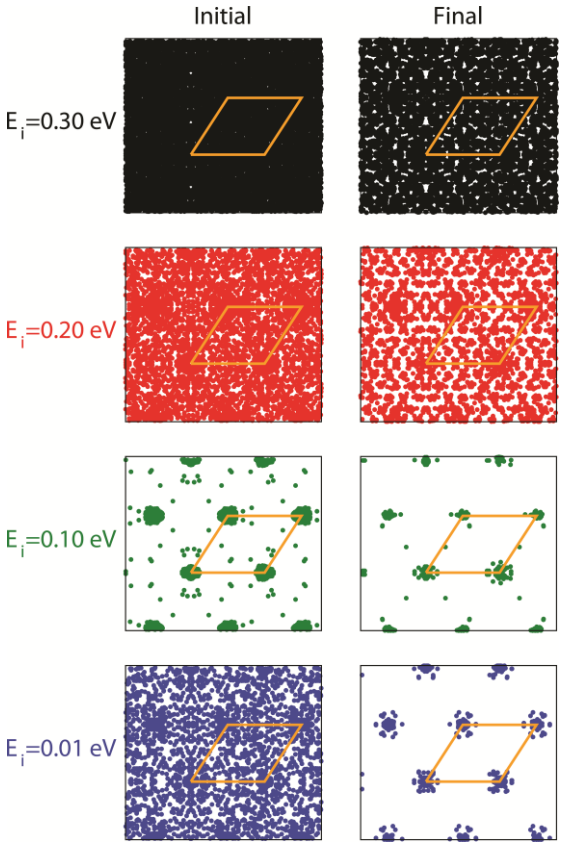

FIG. SI 3. Initial (left panels) and final (right panels) positions of the molecular center of mass for reactive trajectories at impact energies Ei=0.3 eV, 0.2 eV, 0.1 eV, and 0.01 eV (at normal incidence) for H2(v=O,J=O)/Pdo.96Ruo.o4/Ru(0001).

to rationalize the observed increasing reactivity of Ru atoms with increasing number of NN Pd atoms.

DYNAMICS RESULTS

Pd-rich surface alloys

In Fig. 4 we have shown a non-monotonic E_i-dependence of the reactive sticking probability of $H_2(v=0,J=0)$ on $Pd_{0.96}Ru_{0.04}$/Ru(0001). In order to fully understand this behavior, we have analyzed the classical trajectory followed by the molecules in their way towards the surface. In Fig. SI 3 we show the initial (left panels) and final (right panels) position of the molecular center of mass (CM) for all the reactive trajectories at E_i=0.3, 0.2, 0.1, and 0.01 eV. For the highest incidence energy considered (i.e. E_i = 0.3 eV) for which s_0 is high (~ 0.3), the almost uniform distribution of final CM positions shows that dissociation takes place almost everywhere over the unit cell, regardless the position of the most active Ru atoms. For E_i=0.2 eV the scenario is similar to the previous case, but a closer look to Fig. SI 3 shows that the density of dissociation events is slightly higher around the Ru atoms. Though for any E_i value lower than ~ 0.12 eV, H_2 molecules only dissociate around the reactive Ru atoms, the distributions of the initial CM positions of the reactive trajectories for E_i=0.01 eV and 0.1 eV differ significantly from each other. For E_i=0.1 eV almost all the molecules that dissociate were already around the Ru atoms at the beginning of the trajectory, which explains the low sticking probability observed in Fig. 4 for this value of E_i. In contrast, for E_i=0.01 eV even H_2 molecules impinging the surface far from the reactive sites still can find the active Ru sites and dissociate. The lowest panels of Fig. SI 3 clearly show that Pd patches act as *snares* for low energy molecules that remain dynamically trapped near the surface which increases the probability for a molecule of encountering an active Ru site. This is the reason for the increase of s_0 at very low E_i values observed in Fig. 4. This trapping-mediated dissociation mechanism is confirmed by a large number of rebounds near the surface, and long interaction times before dissociation for reactive trajectories at very low incidence energies. In addition, we have verified that for low impact energies ($E_i \leq 0.15$ eV) s_0 scales with total energy [10].

The non-monotonic E_i-dependence of the sticking probability of H_2 molecules discussed above is observed for different alloys Pd_xRu_{1-x}/Ru(0001). In Figs. SI 4 and SI 5 we show the curves $s_0(E_i)$ obtained for various x-values ($0.83 \leq x \leq 1$) and $0 \leq J \leq 3$, for H_2 and D_2 molecules respectively. The results for H_2 and D_2 are very similar to each other, which

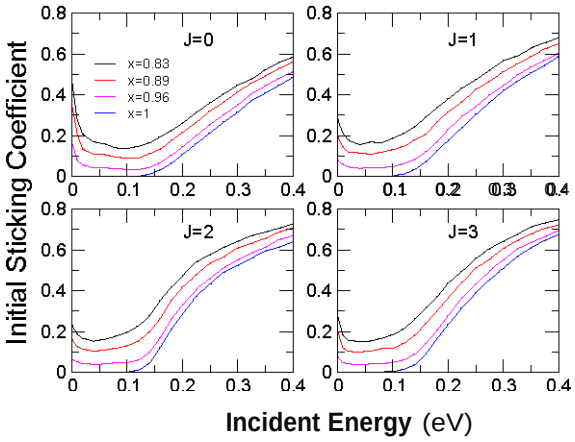

FIG. SI 4. Rovibrational-state-selective initial sticking probability of H_2 (v = 0, J=0, 1, 2, 3) on PdxRul-x/Ru(0001) surfaces with x = 0.83, 0.89, 0.96, and 1, as a function of the impact energy Ei at normal incidence, obtained in QCT calculations.

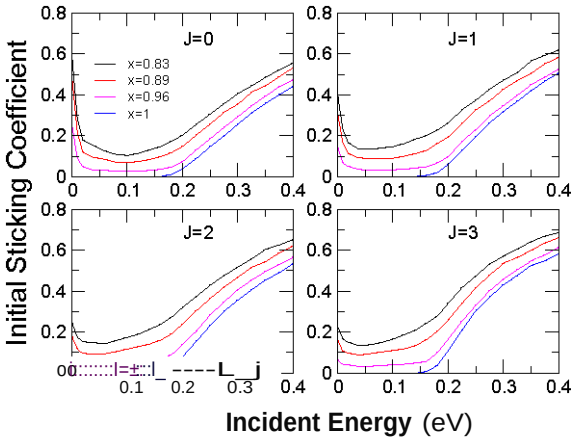

FIG. SI 5. Idem Fig. SI 4 but for D2.

shows that the isotopic effects on the reactive sticking probability for these surface alloys are very small. In addition, rotational effects are also minor at least for $J \lesssim 3$.

In order to compare our theoretical results with experiments (ref. [11] and present work), we have computed $s_0(T_9)$ at room temperature (RT, i.e. for T_9=298 K) as a function of the fraction of Pd atoms in the alloy ($0.83 \lesssim x \lesssim 1$) using Eqs. SI. 13-15 with a = 1 (i.e. the value corresponding to total energy scaling). The results for H_2 and D_2 are summarized in Table I (the former have been also plotted in Fig. 1a). As expected from the results shown in Figs. SI 4 and SI 5, the values of $s_0(T_9$=298K) for H_2 and D_2 are very close to each other.

x	$s_0(T_g = 298K)$ for H_2	$s_0(T_g = 298K)$ for D_2
0.83	1.781×10^{-1}	1.390×10^{-1}
0.89	1.232×10^{-1}	9.238×10^{-2}
0.94	7.339×10^{-2}	5.509×10^{-2}
0.96	4.885×10^{-2}	3.638×10^{-2}
0.97	3.461×10^{-2}	2.566×10^{-2}
0.98	2.688×10^{-2}	1.813×10^{-2}
1.00	3.830×10^{-3}	7.454×10^{-4}

TABLE I. RT-averaged initial sticking probability $s_0(T_g = 298K)$ (see text) for H_2 and D_2 interacting with Pd_xRu_{1-x}/Ru(0001) surface alloys with $0.83 \leq x \leq 1$.

In particular, in both cases, the sharp decrease of s_0 observed in experiments for $x \sim 1$ is well reproduced.

Ru-rich surface alloys

In contrast with the case of Pd-rich surface alloys, dynamic trapping is not likely to take place for Ru-rich alloys because isolated Pd atoms in $Pd_{0.11}Ru_{0.89}$/Ru(0001) do not allow low energy hydrogen molecules (e.g. $E_i \sim 0.01$ eV) to approach the surface below $Z_{CM} \sim 3$ Å (see Fig. SI 6). Thus, assuming that in this case dissociation is a direct activated process, it is possible to estimate the initial sticking probability for different (small) values of the fraction of Pd atoms in the alloy using the following simple model [12]. Let us consider the surface alloys $Pd_{0.11}Ru_{0.89}$/Ru(0001) (x=0.11) and $Pd_{0.14}Ru_{0.86}$/Ru(0001) (x=0.14) modeled by (3×3) and ($\sqrt{7} \times \sqrt{7}$) unit cells respectively (see Fig. SI 7). Within these unit cells one can identify three kind of hexagonal regions: i) centered in a Pd atom (turquoise hexagon), ii) centered in Ru atoms NN of one Pd atom, Ru_{NN}, (red hexagon), and iii) centered in Ru atoms surrounded by Ru atoms (green hexagon). In the case of the ($\sqrt{7} \times \sqrt{7}$) unit cell, there are only regions type i) and ii). Assuming that for $x << 1$ dissociation is a direct activated process, it is reasonable to compute s_0 for x=0.11 ($s_0^{x=0.11}$) and x=0.14 ($s_0^{x=0.14}$) as follows [12]:

$$s_0^{x=0.11} = \frac{1}{9} s_0^{Pd} + \frac{2}{9} s_0^{Ru_{NN}} + \frac{2}{9} s_0^{Ru} \qquad \text{(SI. 16)}$$

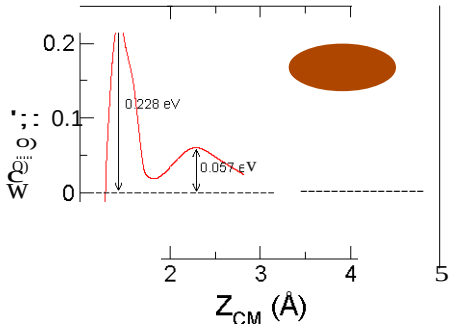

FIG. SI 6. Potential energy along a DP of H_2 on Pdo$_{11}$Ruosg/Ru(0001) (for a fcc-topPd-hcp configuration) as a function of the height of the molecule above the surface, *ZcM·*

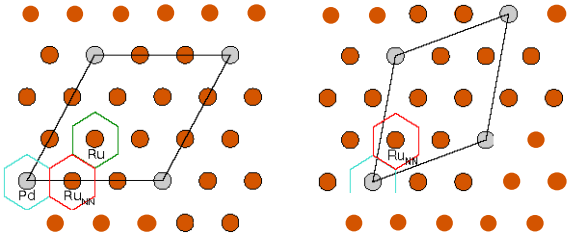

FIG. SI 7. Schematic representation of the (3x3) (left) and (.,;7 x .,;7) (left) unit cells employed to model the PdonRuosg/Ru(OOOl) and Pdo14Ruos6/Ru(0001) surfaces, respectively.

$$s_0^{x=0.14} = \frac{1}{7}\, s_0^{Pd} + \frac{6}{7}\, s_0^{Ru_{NN}} \qquad \text{(SI. 17)}$$

In Eqs. SI. 16 and SI. 17, Sd, *suNN,* and *s u* are the *parti al* sticking probabilities corresponding to trajectories starting within the regions type i), ii), and iii) respectively.

Given that we are interested in a gas of molecules at RT, sd can be neglected because most of the molecules have translational energies below the dissociation threshold on Pd atoms (Ei 0.12 eV). In addition, su can be approximated by the sticking probability of molecular hydrogen on pure Ru(0001). Kroes and co-workers have computed the latter probability as a function of Ei for H_2 (v=0,1=0) using both quantum (Q) [13] and QCT calculations [14]. These results are shown in the inset of Fig. SI 8. Finally, we have approximated *s uNN* (Ei) by s u(Ei+8meV) because the early barrier found for the fcc-topRu-hcp molecular configuration on pure Ru(0001) , decreases by rv 8 meV on top of *RuNN* atoms in rich-Ru surface alloys (see Fig. 5).

Fig. SI 8 shows s_0 (Ei) *!B(Ei)* obtained in this way for *x=O* (i.e. pure Ru(0001)), x=O.ll,

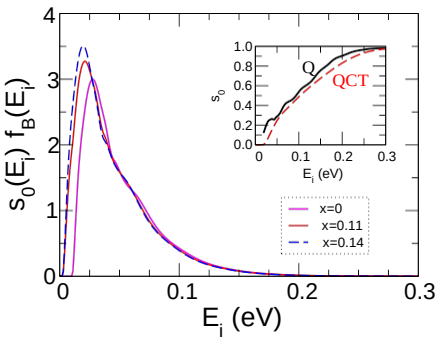

FIG. SI 8. RT-weighted initial sticking probability as a function of the initial impact energy at normal incidence, $s_0(E_i)$ $f_B(E_i)$, for $H_2(v=0,J=0)/Pd_xRu_{1-x}/Ru(0001)$ with x = 0, 0.11, and 0.14 (see text). Inset: quantum (Q, full black line) and quasi-classical trajectory (QCT, dashed red line) $s_0(E_i)$ curves for $H_2(v=0,J=0)/Ru(0001)$, taken from refs. [13] and [14] respectively.

and x=0.14 for T_g =298 K and using the Q sticking curve $s_0(E_i)$ for $H_2(v=0,J=0)/Ru(0001)$ (extrapolated linearly for $E_i \rightarrow 0$). In this case we have used Eqs. SI. 13 and SI. 14 with α=0 because for Ru(0001) and Ru-rich alloys we have assumed that s_0^{Ru} scales with normal energy as expected for direct dissociation over an early activation barrier. The use of Q $s_0(E_i)$ curve instead of the QCT one is because quantum effects are particularly important near the threshold where the contribution to $s_0(T_g)$ is the highest.

Fig. 1a shows that for Ru-rich surface alloys, $s_0(T_g=298K)$ (i.e. the area below the curve displayed in Fig. SI 8) presents a scarce dependence on the Pd concentration, x. In fact, the presence of isolated unreactive Pd atoms in Ru-rich $Pd_xRu_{1-x}/Ru(0001)$ alloys is slightly overcompensated by the increased reactivity of their NN Ru atoms. Though the use of QCT sticking results [14] gives rise to values of $s_0(T_g)$ smaller than with the Q ones [13], the small x-dependence for $0 \leq x \leq 0.14$ remains unchanged.

[1] P. Nieto, D. Barredo, D. Farías and R. Miranda, *J. Phys. Chem. A*, 2011, **115**, 7283.

[2] P. Nieto, D. Farías, R. Miranda, M. Luppi, E. Baerends, M. Somers, M. van der Niet, R. Olsen and G. Kroes, *Phys. Chem. Chem. Phys.*, 2011, **13**, 8583.

[3] N. Rougemaille, F. E. Gabaly, R. Stumpf, A. Schmid, K. Thürmer, N. Bartelt and J. de la Figuera, *Phys. Rev. Lett.*, 2007, **99**, 106101.

[4] B. Santos, J. M. Puerta, J. I. Cerda, T. Herranz, K. F. McCarty and J. de la Figuera, *New J. Phys.*, 2010, **12**, 023023.

[5] B. Poelsema and G. Comsa, *Scattering of Thermal Energy Atoms from Disordered Surfaces. Springer Tracts in Modern Physics Vol. 115*, Springer-Verlag, Berlin1989.

[6] D. Farías and K. H. Rieder, *Rep. Prog. Phys.*, 1998, **61**, 1575.

[7] G. Comsa and R. David, *Surf. Sci. Rep.*, 1985, **5**, 145.

[8] H. F. Busnengo, C. Crespos, W. Dong, J. C. Rayez and A. Salin, *J. Chem. Phys.*, 2002, **116**, 9005.

[9] B. Hammer and J. K. Nørskov, *Nature*, 1995, **376**, 238.

[10] C. Díaz, H. F. Busnengo, F. Martín and A. Salin, *J. Chem. Phys.*, 2003, **118**, 2886.

[11] H. Hartmann, T. Diemant, A. Bergbreiter, J. Bansmann, H. Hoster and R. J. Behm, *Surface Science*, 2009, **603**, 1439.

[12] M. Ramos, M. Batista, A. Martínez and H. Busnengo, *Springer Series in Surface Science 50. Dynamics of Gas-Surface Interactions*, Springer2013.

[13] J. K. Vincent, R. A. Olsen, G. J. Kroes, M. Luppi and E. J. Baerends, *J. Chem. Phys.*, 2005, **122**, 044701.

[14] M. Wijzenbroek and G.-J. Kroes, private communication.